Proceedings of ERAD (2004): 94–98 © Copernicus GmbH 2004

ERAD 2004

Mesoscale processes and energetics of fastex secondary cyclogenesis

C. Heyraud, A. Protat, and Y. Lemaître

Centre d'Etude des Environnements Terrestre et Planétaires (CETP), Vélizy, France

1 Introduction

During FASTEX (January and February 1997), 19 frontal cyclones at different stages of development have been sampled using airborne facilities (dropsondes and 2 dual-beam Doppler radars). Thanks to this important data set, the three-dimensional dynamic and microphysical structure of the North–Atlantic frontal cyclones is documented and the multi-scale processes are investigated in the present paper. Previous studies conducted at the CETP on the a bent-back warm front case of FASTEX (Intensive Observing Period 16, IOP16) documented the dynamic and thermodynamic structure at all scales of motions. Hypotheses deduced from recent theoretical studies of the dynamics of frontal cyclones have been evaluated. In this context, the conceptual scheme of secondary cyclones of Browning (1997) has been validated. Bouniol et al. (2001) underscore the crucial role played by specific mechanisms in the intensification of this typical secondary low:

- upper and low level coupling processes (see for instance Thorncroft and Hoskins, 1990).
- low forcing of the large scale environment (see for instance Bishop and Thorpe, 1994a, b).
- instability mechanisms: conditional symmetric instability (see for instance Balasubramian and Yau, 1994).
- importance of vorticity stretching in vorticity production at the low center.

The present study attempts to evaluate the degree of generality of these results and the evolution of the processes during the life cycle. For this purpose, six cases at different stages of development are investigated.

This study is based on the estimation of diagnostic parameters at mesoscale, such as production of vorticity, energetic conversion, and impact of cyclogenesis on the environment in terms of heat budgets. All these points are discussed below.

Correspondence to: C. Heyraud
(catherine.heyraud@cetp.ipsl.fr)

2 Data and methods

The measurement have been collected by two aircraft (NOAA P-3 and NCAR Electra) bearing the airborne Doppler radars and the C-130 aircraft from which dropsondes were launched every 70 km within the cyclones.

The combination of the measurements allows to document the three-dimensional wind field in both the precipitating and non-precipitating areas using the MANDOP analytical method (Scialom and Lemaître, 1990) adapted by Montmerle and Lemaître (1998) to include the dropsonde information in the variational process. The 3-D thermodynamic fields (pressure and temperature) are retrieved using the analytical method developed by Protat et al. (1998). The water vapor field is retrieved using the dropsonde measurements (Bouniol et al., 1999).

3 Six selected FASTEX cases

During FASTEX different kinds of meteorological events have been sampled from the weak frontal wave to the explosive cyclogenesis. Six cases have been selected to conduct this study: IOP1, IOP5, IOP11, IOP12, IOP16, IOP17.

- IOP1 (10 January) is a frontal fracture, the cloud head and dry intrusion are observed.
- IOP5 (22 January) and IOP11 (5–6 February) are 2 primary cyclones forming on a frontal wave. IOP11 is a deepening primary cyclone with training cold and warm fronts whereas IOP5 is not developing.
- IOP12 (9 February) is an explosive cyclogenesis, a "bomb-like" deepening in mature phase (roughly -54 mb in 24 h) as described by Lemaître et al. (1999).

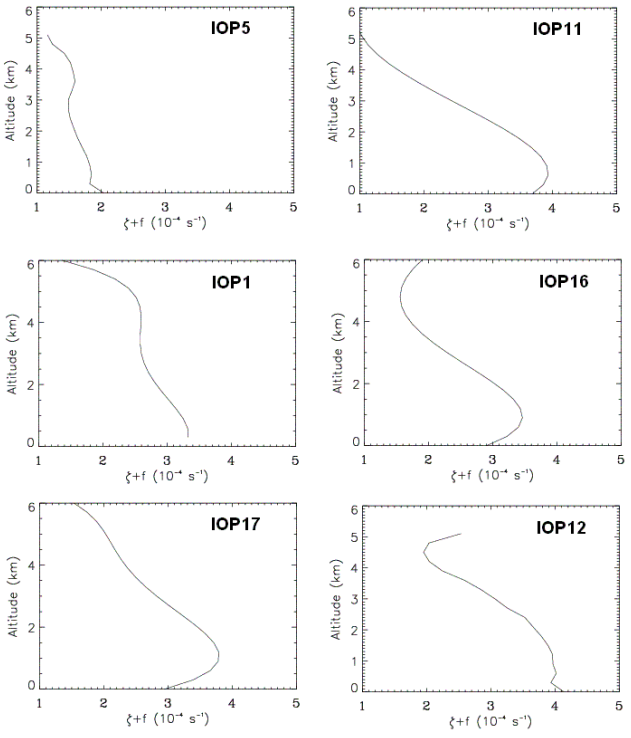

Fig. 1. Mean vertical profile of the vertical vorticity component ($10^{-4}s^{-1}$) for IOPs 5, 11, 1, 16, 17, 12.

– IOP16 sampled on 17 February 97 is a fast moving rapidly-deepening secondary wave with emerging cloud head and distinct dry intrusion.

– IOP17 (19 February) is the "FASTEX cyclone", this is an explosive deepening cold wave characterised by a 40 mb deepening in 24 h.

According to the conceptual scheme of a frontal cyclone life cycle (Shapiro and Keyser, 1990), we classify qualitatively the cyclones: IOP5 and 11 are incipient frontal cyclones, IOP5 is not developing whereas IOP11 is in development. IOP1 is a "frontal fracture", IOP16 is a bent-back warm front. IOP17 and IOP12 are warm-core seclusion; IOP12 is no more deepening. All the results will be discussed following this specific order.

The 3-D dynamic and thermodynamic characteristics of these FASTEX cyclones have been retrieved. Thanks to this important data set, the ambition addressed here is to document the characteristics of the six FASTEX cases and to overhead the role of the development stage on these characteristics.

4 Production of vorticity

The purpose of this section is to evaluate the evolution of the cyclogenesis and to diagnose the processes involved in this evolution in terms of the absolute vorticity:

$$\vec{\omega}_a = \nabla \wedge \boldsymbol{V} + f\boldsymbol{k} = \eta\, \boldsymbol{i} + \xi\, \boldsymbol{j} + (\zeta + f)\boldsymbol{k} \qquad (1)$$

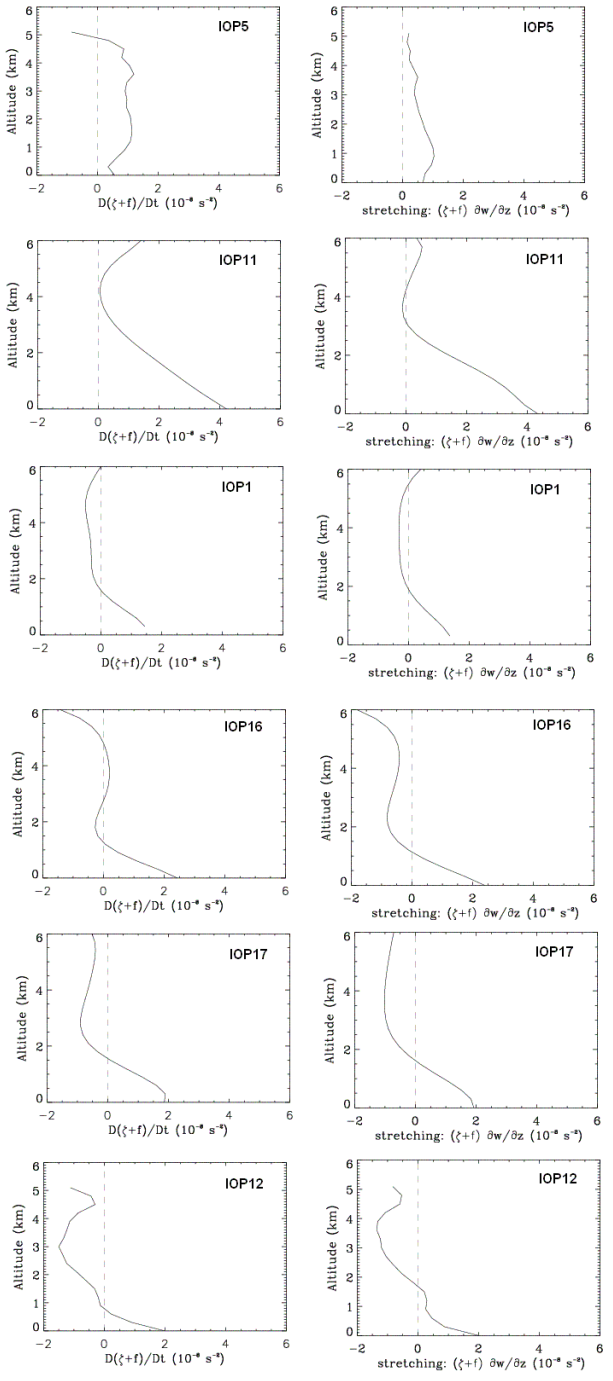

Fig. 2. Mean vertical profile of the absolute vertical vorticity evolution (first column) and stretching term (second column) for IOPs 5, 11, 1,16,17,12 ($10^{-8}s^2$).

$$\frac{D(\zeta + f)}{Dt} = \eta\frac{\partial w}{\partial x} + \xi\frac{\partial w}{\partial y} + (\zeta + f)\frac{\partial w}{\partial z} + \frac{\partial Fy}{\partial x} - \frac{\partial Fx}{\partial y} - \frac{1}{\rho^2}\left(\frac{\partial \rho}{\partial x}\frac{\partial p}{\partial y} - \frac{\partial \rho}{\partial y}\frac{\partial p}{\partial x}\right) - (\zeta + f)\frac{\nabla \boldsymbol{\rho}}{\rho}.V \qquad (2)$$

where (u,v,w) are the wind components, (η,ξ,ζ+f) are the absolute vorticity components, f is the coriolis parameter, F is the friction and ρ the density.

The quantification of the different terms of this equation indicates that only the stretching $(\zeta + f)\frac{\partial w}{\partial z}$ and tilting $(\eta\frac{\partial w}{\partial x} + \xi\frac{\partial w}{\partial y})$ terms have significant values (first and second terms of (2)). The other terms are negligible. The mean vertical profiles are computed in a $170\times170\,\mathrm{km}^2$ box centred on the maximum vorticity for all the cases. This vorticity maxima is located in the cyclonic circulation area observed in the low tropospheric layers (1.5 km).

Figure 1 shows the vertical component of vorticity for the six IOPs. For all the cases it is positive and the maximum (3–4 $10^{-4}\,\mathrm{s}^{-1}$) is located at around 1 km altitude. This result confirms the presence of an intense cyclonic circulation in this area.

The quantification of the different components of (2) allows to diagnose the processes involved in the vorticity evolution for the studied cases.

Figure 2 shows the Lagrangian evolution of this parameter and the stretching term.

These figures highlight a production of vorticity in the low tropospheric layers (below 2 km altitude) for the 6 cases except for IOP5. The vorticity production is typically $2.10^{-8}\mathrm{s}^{-1}$. For IOP5, the production is weaker and for IOP11 it is two times larger. An explanation could be that IOP5 and IOP11 are frontal waves and IOP5 is a non developing one and IOP11 is deepening. As shown by the strong similarity of the production and of the stretching term profiles in Fig. 2, the evolution of vorticity is mostly driven by the stretching term for all the cases.

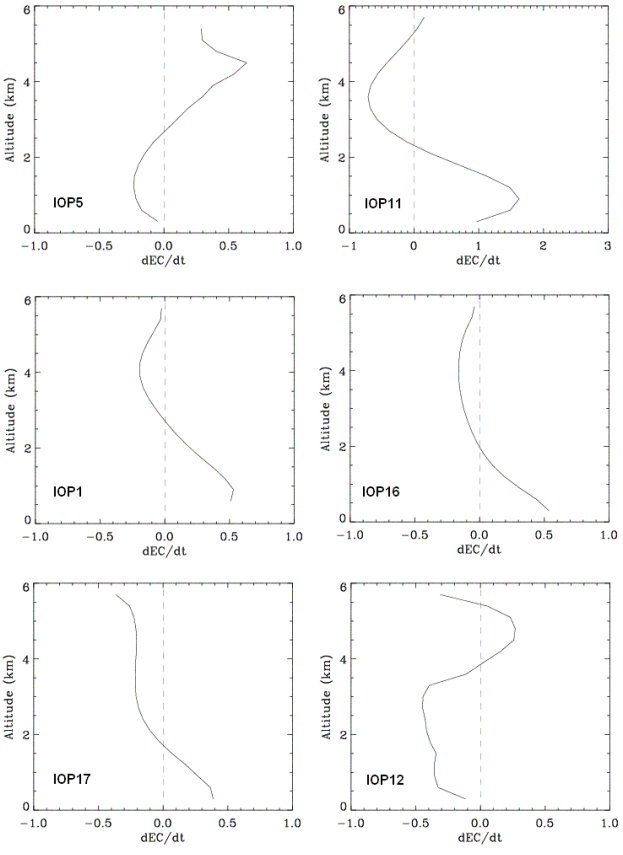

Fig. 3. Mean vertical profile of kinetic energy production ($10^{-2}\mathrm{J.k}^{-1}\mathrm{s}^{-1}$) for IOPs 5, 11, 1, 16, 17, 12.

5 Energetic conversion

The aim of this section is to answer the following question: what are the conversion mechanisms and the associated instabilities systematically involved in the development of secondary cyclogenesis?

The production/dissipation of kinetic energy is written as:

$$\overline{\frac{\partial Ec}{\partial t}} = \frac{g}{\theta 0}\overline{w'\theta'} - \frac{1}{\overline{\rho}}\overline{\boldsymbol{V}.\boldsymbol{\nabla}p'} - \overline{(u'+v'+w')\boldsymbol{V}'.\boldsymbol{\nabla}(\overline{u}+\overline{v}+\overline{w})} - \overline{\boldsymbol{V}.\boldsymbol{\nabla}Ec} \quad (3)$$

where the over-bar denotes the average over the whole retrieval domain and the prime denotes the deviation from the average. θ is the potential temperature, the wind vector V components are (u,v,w).

The first term on the right hand side of (3) is the vertical heat flux, the second term the production due to the pressure term; the third term the Reynolds Stress (RS) and the last one the advection term. The Reynolds Stress reveals the energy exchange between the different scales: larger and "perturbation" scale by means of energetic conversion associated with symmetric instability and barotropic instability. These terms can be expressed as in (4). The first term of (4) relates to the horizontal Reynolds Stress (HRS) relevant to the presence of barotropic instability and the second the vertical Reynolds Stress (VRS) relevant to the symetric instability.

$$RS = \left[\overline{u'u'}\overline{\frac{\partial u}{\partial x}} + \overline{v'v'}\overline{\frac{\partial v}{\partial y}} + \overline{u'v'}\overline{(\frac{\partial u}{\partial y}+\frac{\partial v}{\partial x})} + \overline{u'w'}\overline{\frac{\partial w}{\partial x}} + \overline{v'w'}\overline{\frac{\partial w}{\partial y}}\right] + \left[\overline{u'w'}\overline{\frac{\partial u}{\partial z}} + \overline{v'w'}\overline{\frac{\partial v}{\partial z}} + \overline{w'w'}\overline{\frac{\partial w}{\partial z}}\right] \quad (4)$$

Figures 3 and 4 show the mean vertical profiles of the kinetic energy and the two components of the Reynolds Stress (HRS and VRS) for the six IOPs calculated in the previous $170\,\mathrm{km}^2$ box.

For the cases in development, the kinetic energy of the perturbation tends to increase in the low level (below 2km) and decrease in the upper level (see Fig. 3). On the contrary the kinetic energy for IOP5 and IOP12 is decreasing in the low levels which confirms the non developing stage of IOP5 and suggesting that IOP12 had reached its maximum growing phase previously. The most important production is observed for IOP11.

From Fig. 4 it is clearly seen that in the low layer of atmosphere the positive tendency of the horizontal Reynolds stress overheads systematically the presence of barotropic conversion of energy, while at higher height there is a clear signature of symmetric conversion.

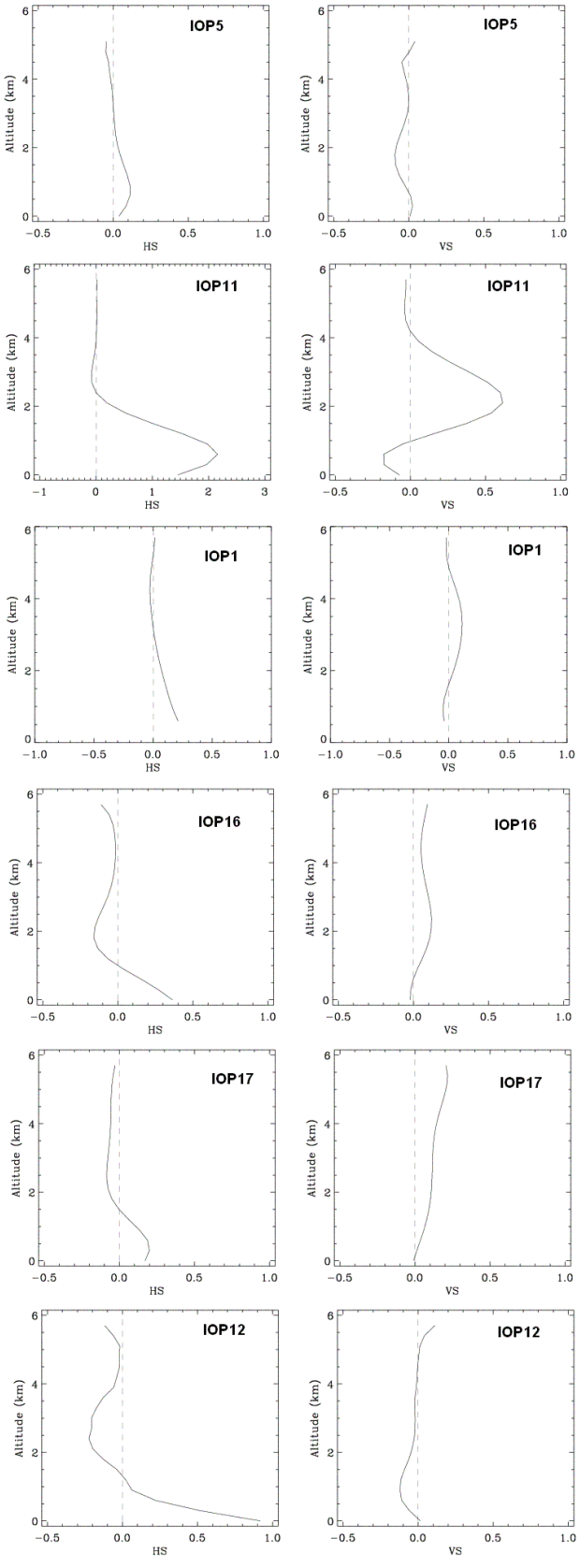

Fig. 4. Mean vertical profile of HRS (first column) and VRS (second column) (10^{-2}J.kg^{-1}s^{-1}) for IOPs 5, 11, 1, 16, 17, 12.

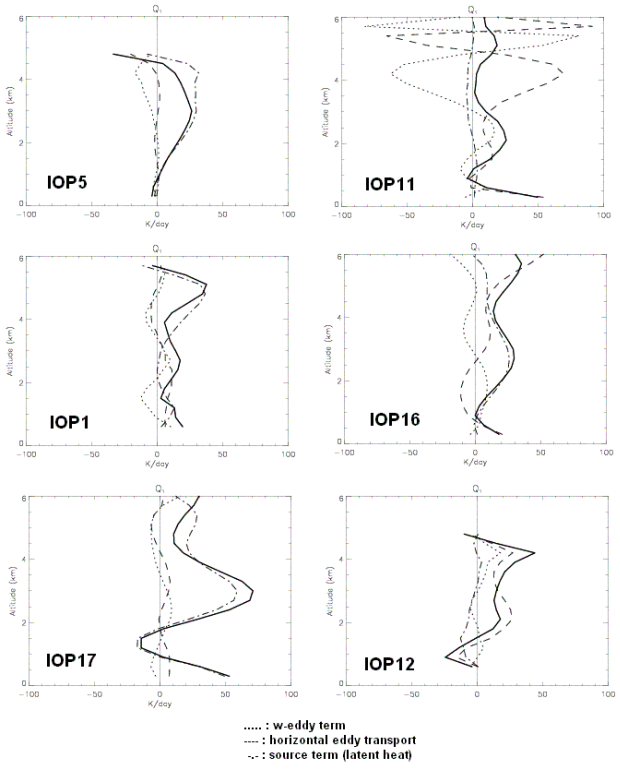

Fig. 5. Vertical profile of the heat source on mesoscale for IOPs 5, 11, 1, 16, 17 and 12 and the contribution of the different processes (w-eddy term, horizontal eddy transport, source term).

6 Heat Budget of the cyclones

In this section, the impact of cyclogenesis on the environment is quantified in terms of net heating/cooling using the apparent heat budget (Q_1):

$$Q_1 = \bar{\pi}\ (\boldsymbol{V} - \boldsymbol{C})\ .\nabla\bar{\boldsymbol{\theta}} \tag{5}$$

where π is the nondimensional pressure,θ the potential temperature, C the advection speed vector of the moving frame of reference, and the over-bar denotes the average over the whole retrieval domain. This equation may also be rewritten as:

$$Q_1 = -\frac{\bar{\pi}}{\bar{\rho}}\overline{\nabla.\left(\bar{\rho}\,\theta'\boldsymbol{V'}\right)} + \bar{\pi}\ \overline{S\,(\theta)} + D_{Q_1} \tag{6}$$

Where the prime denotes the deviation from the average, D_{Q1} is a subgrid-scale diffusion term (computed in the present case but always negligible), and $S(\theta)$ is a source term reflecting diabatic heating. The first term on the right-hand side of (6) is the eddy heat flux convergence term, reflecting warming/cooling of the environment of the cyclone due to scales resolved by the analysis or smaller. An estimate of the latent heat term is obtained by computing the eddy heat flux convergence term in (6) and subtracting it to the Q_1 computed using (5). The mean vertical profile of Q_1 is depicted in Fig. 5.

The positive tendency of the apparent heat budget indicates that the cyclogenesis tends to warm the atmosphere. The heating intensity appears to be related to the intensity of the cyclone. For instance IOP17 defined as the most intense FASTEX cyclogenesis result in the strongest warming (50 K/day).

Signatures of cooling are also identified in the low layers of the troposphere except for IOP1 and IOP16.

A mid-altitude peak is also present in most of the cases, it is associated to the cloud head and it is due to the release of latent heat. This source term seems to play a role more and more important for the developing cases (IOP11 to IOP17) whereas the eddy transport terms seems to play a role less and less important.

The shapes of the profiles seem to be related to the stage of development and the structure of the cyclogenesis (presence of cloud head).

7 Conclusion

These results show the existence of systematic behaviour of secondary cyclogenesis in terms of production of vorticity, energetic conversion and global impact on the environment.

However our short-term perspective is to widen this study on other diagnostic parameters such as potential vorticity, moist potential vorticity, and impact of cyclogenesis on the environment in terms of momentum transport. The non-hydrostatic méso-NH model initialized by the ECMWF analysis is presently used and two sub-domains are nested in order to increase the resolution of the simulation. After validation of a FASTEX case simulation using the observation dataset, the evolution of the diagnostic parameters will be performed during an entire life cycle and compared to the different phase of the life cycle sampled during FASTEX.

References

Balasubramian, G. and Yau, M. K.: Baroclinic instability in a Two-layer Model with Parametrized Slantwise Convection, J. Atmos. Sci., 26, 570–583, 1994.

Bishop, C. H. and Thorpe, A. J.: Frontal wave stability during moist deformation frontogenesis. Part I: Linear wave dynamics, J. Atmos. Sci., 51, 852–873, 1994a.

Bishop, C. H. and Thorpe, A. J.: Frontal wave stability during moist deformation frontogenesis. Part II: The suppresion of non-linear wave development, J. Atmos. Sci., 51, 873–888, 1994b.

Bouniol, D., Protat, A., and Lemaître, Y.: Mesoscale dynamics of a deepening secondary cyclone (FASTEX IOP16): Three-dimensional structure retrieved from dropsonde data, Quart. J. Roy. Meteor. Soc., 125, 3535–3562, 1999.

Bouniol, D., Lemaître, Y., and Protat, A.: Upper and lower tropospheric coupling processes involved in the FASTEX IOP16, Quart. J. Roy. Meteorol. Soc., submitted, 2001.

Browning, K. A.: Mesoscale aspects of extratropical cyclones: an observational perspective, Bergen post-conference book, ED. M. Shapiro. American Meteorological Society, Boston, Mass., 1997.

Lemaître, Y., Protat, A., and Bouniol, D.: Pacific and Atlantic "bomb-like" deepenings in mature phase: A comparative study, Quart. J. Roy. Meteor. Soc., 125, 3513–3534, 1999.

Montmerle, T., and Lemaître, Y.: 3D variational data analysis to retrieve thermodynamical and dynamical fields from various nested wind measurements, J. Atmos. Oceanic Technol., 15, 360–379, 1998.

Protat, A., Lemaître, Y., and Scialom, G.: Thermodynamic analytical fields from Doppler radar data by means of the MANDOP analysis, Quart. J. Roy. Meteorol. Soc., 124, 1633–1668, 1998.

Scialom, G. and Lemaître, Y.: A new analysis for the retrieval of the three-dimensional wind field from multiple Doppler radars, J. Atmos. Oceanic Technol., 7, 640–665, 1990.

Shapiro, M. A. and Keyser, D.: Fronts, jet-streams and Tropopause, In Extratropical cyclones: the Erik Palmen Memorial Volume, C. W Newton and E. O. Holopainen (Eds), American Meteorological Society, 167–191, 1990.

Thorncroft, C. D. and Hoskins, B. J.: Frontal cyclogenesis, J. Atmos. Sci., 47, 2317–2336, 1990.